Evaluation and improvement of digital image correlation uncertainty in dynamic conditions

Emanuele Zappa, Ali Matinmanesh *, Paolo Mazzoleni

Politecnico di Milano, Dipartimento di Meccanica, via La Masa 1, 20156 Milano, Italy

Article history:
Received 31 October 2013
Received in revised form
16 January 2014
Accepted 17 March 2014

1. Introduction

Digital Image Correlation [1,2] is a powerful technique, which has been mostly used in static applications. More recently, in a variety of studies, DIC has been exploited also in dynamic applications. However, reviewing the literature reveals that further investigations of DIC performances in generic dynamic conditions need to be done. The performances of DIC technique depend on a set of static and dynamic parameters; the formers include image resolution and blurring, lighting conditions and processing parameters. As for the dynamics, the motion parameters (mainly the instantaneous velocity) and the shutter time are usually considered relevant in image-base measurement uncertainty assessment [3,4].

Dealing with a moving target causes a motion effect (i.e. blurring) on the acquired images. This factor is an important source of measurement uncertainty. Therefore, the present study aims to evaluate and improve DIC uncertainty in dynamic conditions in the case of translating target. The study focuses on 2D DIC. In the case of 3D DIC similar problems arise, and therefore a complete understanding of two dimensional conditions will be of great help for further studies which deal with 3D conditions.

The whole work can be divided into two main parts. The first part aims to analyze the effect of dynamics on the DIC uncertainty by proposing numerical and experimental approaches. The numerical approach is based on implementing two innovative methods to simulate the motion effect on a reference image. These numerical methods allow keeping all the other uncertainty sources under control and exploring the effect of dynamics. The performances of the two methods are then evaluated in different dynamic conditions. With these models and a given static image of the target, it is possible to simulate the dynamic test and create a set of images that simulate the ones that would be obtained from a real test, with a known imposed vibration law. The simulated image sets are analyzed by means of DIC technique and the discrepancy between the imposed and the estimated time histories is utilized to estimate the uncertainty. The simulations are successively validated by conducting several harmonic vibration tests.

In the second part of the study a numerical technique is proposed to estimate the motion effect present in an acquired image. This technique gives two main advantages. First, since the motion effect itself has a known influence on the uncertainty of measurement (thanks to the first part of the study), it is possible to predict the DIC's uncertainty by just having an acquired image.

* Corresponding author. Tel.: +39 3801812779.
E-mail address: ali.matin@mail.polimi.it (A. Matinmanesh).

Second, this numerical technique is used to improve the performances of DIC in dynamic applications.

1.1. State of the art

Studies related to DIC uncertainty in static applications started early on and remarkable advances have been made in this area in the recent years [5–13]. The available literature in the case of static DIC applications is wide, as summarized in [14]. Different approaches to DIC uncertainty analysis have been proposed and implemented in the literature.

Some efforts have been made to theoretically estimate the DIC uncertainty [15–17]. In 2009, groups of researchers presented theoretical formulae defining the effect of noise in the intensity pattern, image contrast and interpolation method on both bias and variability in one-dimensional motion measurements [18,19]. Wang et al. [20] used basic equations for stereo-vision with established procedures for camera calibration, to provide error propagation equations that can be used to determine both bias and variability in a general 3D position and successively experimentally validated them [21]. In another approach a group of studies investigate the DIC uncertainty by creating a set of synthetic images [22–26].

Although, the above mentioned works were concerned with static cases, the implementation of DIC did not remain limited to static applications. Recently, in a group of studies, DIC has been implemented for modal shape recognition and vibration analysis [27–36], while a group of researchers focused on defining reference materials for dynamic conditions [37–39].

In a previous paper the authors focused on systematic evaluation of the uncertainty of DIC in dynamic conditions [14]. In this work, further investigations have been done in this regard by introducing an improvement motion simulation technique and above all, proposing a deconvolution-based numerical technique capable of decreasing the bias and random components of error in DIC measurements in dynamic conditions (Section 4).

2. Methods

In order to analyze the uncertainty of DIC in dynamic conditions, sets of reference images of a target are required; the current section describes the numerical and experimental approaches applied to obtain these sets of images. Section 2.1 addresses the issue of sub-pixel shifting using Fourier Transform since this operation is required in the proposed methods for motion effect simulation (Section 2.2). Then two methods to simulate the motion effect are discussed in detail. They will be implemented in different conditions in order to estimate the uncertainty of DIC in dynamic cases. In Section 2.3, details of the experimental tests are explained which were carried out not only to validate the simulations but also to perform a systematic uncertainty assessment in real conditions.

2.1. Sub-pixel shift using DFT

The simulation of the pure translation of the target is the first step towards simulating the motion effect, as explained in Section 2.2. Among several techniques introduced in this regard, Fourier shifting method is claimed to be the optimum sub-pixel shifting technique [40]. This method is composed of three steps. The image is first transformed into the frequency domain via Discrete Fourier Transform (DFT). Then, a linear phase shift (i.e. with a phase shift linearly proportional to the spatial frequency) is applied in the complex plane. The amount of added phase determines the amount of the spatial shift. Finally the image is transformed back to the spatial domain via an Inverse Discrete Fourier Transform. The transforms are done via 1D DFT/IDFT of a single row or a single column at a time [40]. Note that, applying a linear phase shift to the image in frequency domain is equivalent to convolving the image with an impulse function with impulse at time different from zero.

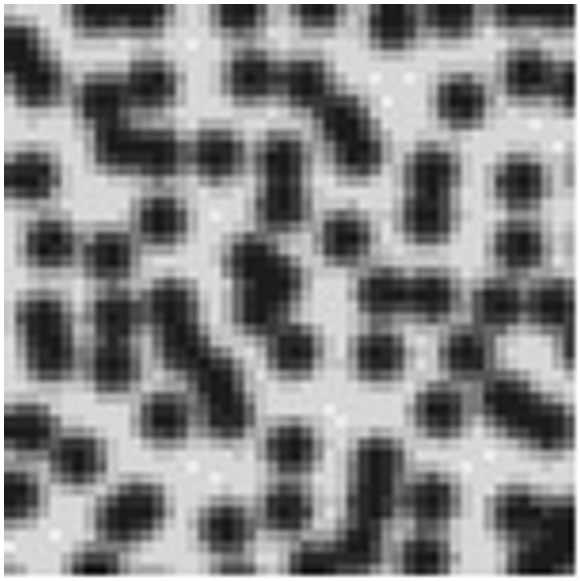

Fig. 1. Reference image.

Fig. 1 shows the reference, un-deformed speckle pattern image used in all of the simulations. It is a 2000×2000 pixels speckle pattern with grain size of 4 pixels.

2.2. Generation of images with motion effect

As discussed already in the last section, convolving the image with impulse function is a recognized method to simulate the sub-pixel shifting. In order generate images with motion effect, two main techniques can be considered. The first technique is the square pulse method which is based on convolution of reference image with a square pulse (previously introduced by authors in [14] to simulate the motion effect for DIC uncertainty in dynamic condition). The second one is the averaging method which will be explained in Section 2.2.2. As demonstrated later, in some dynamic cases the latter better simulates the real conditions.

2.2.1. Motion effect simulation using square pulse

The numerical method for motion effect simulation using square pulse is based on convolution of the reference image with square pulse [14]. Therefore for simulating an acquired image in any dynamic condition the width of the square pulse 'w' and the corresponding shift 'a' have to be determined. Fig. 2 shows a square pulse function $g(x)$ and the two corresponding parameters 'w' and 'a'.

Moreover, convolution in space domain is equivalent to multiplication in spatial frequency domain. The technique to simulate the motion effect in horizontal direction proposed in [14] is to calculate the DFT of each row of the image and multiply it by DFT of square pulse and finally calculate the inverse DFT of the product. The same procedure can be followed in operating with image columns to simulate a vertical motion effect. We name this procedure as the numerical method of motion effect simulation. It should be mentioned that if we convolve the image with shifted

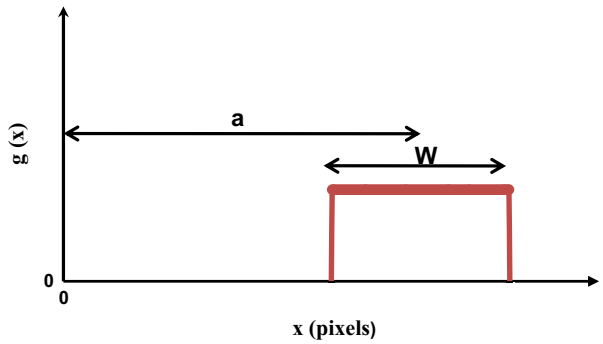

Fig. 2. Square pulse $g(x)$ with parameters 'w' (width of the square pulse) and parameter 'a' (shift).

square pulse in space domain we will get a shifted image with motion effect.

In the case of rigid motion, parameter 'w' is the length of the path covered by the target during the exposure time and the parameter 'a' is equivalent to the net displacement of the target with respect to the reference image at the middle of the exposure time [14]. The limitation for using the numerical method is that the square pulse length parameter 'w' can be only an integer value but there is a need to simulate the motion with sub-pixel accuracy. Therefore an analytical method was proposed in [14]. The analytical method is based on creating the Fourier Transform of the square pulse directly in frequency domain without the need to work in space domain; this allows handling the motion effect also with sub-pixel amplitude. The continuous Fourier Transform of square pulse (i.e. sinc function) is directly multiplied by the DFT of each row of the reference image and the inverse DFT of the product is computed.

2.2.2. Motion effect simulation by averaging the shifted images

The square pulse simulation technique implies the velocity of motion to be constant during the exposure time. This is due to the shape of the square pulse, which is constant over its width. In cases in which this hypothesis (constant velocity during the exposure time) is not valid, a second technique based on image averaging, can be exploited. As an example in the case of sinusoidal motion, the averaging approach is capable of simulating the reality much better than the square pulse method. The reason is that when the object is close to the harmonic pattern peaks the velocity considerably changes. Moreover, the averaging method is simple and based on the approved method of FFT shift [40].

In the case of zero mean displacement (motion effect only), both methods are applicable if the velocity is considered to be constant. Applying the averaging method is even more straightforward than the previously presented one. The procedure consists of two steps. First step is to generate 'N' shifted images during the exposure time, each being displaced by 'a_j' pixel (px) with respect to the reference image, where 'a_j' is the shift value in pixels. In the case of zero mean displacement (motion effect only) 'a_j', assumes values from $(-(w/2))$ to $(+(w/2))$ in (w/N) steps. 'w' is the length of the path covered by the target during the exposure time and 'N' is number of samples. The second step is to average these generated images and obtain a single image. This image is the simulated version of the real image of the target as recorded by the camera. By increasing the number of samples 'N', we will have better estimation of the average image.

In the case of sinusoidal vibration, velocity change during the exposure time is not negligible. The case is even worse if we are dealing with longer exposure time with respect to the period of harmonic displacement law. Therefore in such conditions, the

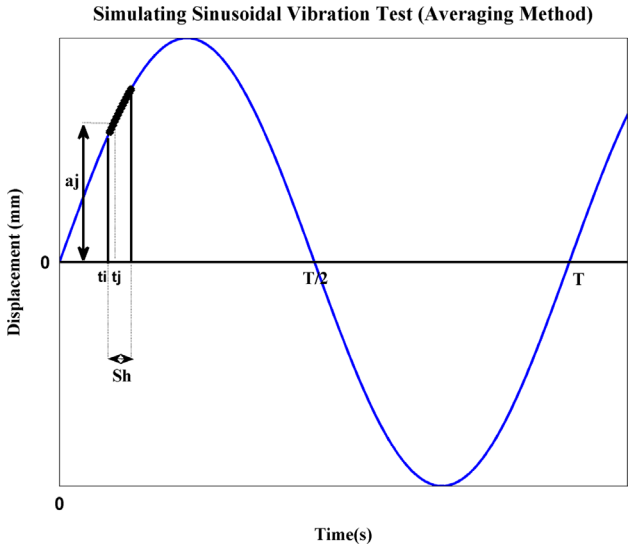

Fig. 3. Simulating the sinusoidal vibration test. Parameters 'A' and 'T' represent amplitude and period of the sinusoidal displacement law. Acquisition starts at $t=t_i$ and ends 'sh' (exposure time) seconds later at $t=sh+t_i$. Parameter 'a_j' is the shift value used to generate one of the shifted images during the exposure time where 't_j' is the corresponding time.

averaging method is expected to be more reliable than the square pulse method. Later on, in Section 3.2 this statement will be proved.

Fig. 3 helps understand how the averaging method is implemented in order to simulate ith image, acquired at $t=t_i$. This acquisition takes 'sh' seconds and ends at $t=t_i+sh$, in which 'sh' represents the exposure time (shutter time). The first step of simulation is to generate 'N' shifted images during the exposure time, each having a shift value calculated as follows:

$$\textit{object's displacement} \quad a_j = A\ \sin\left(\tfrac{2\pi}{T}(t_j)\right) \tag{1}$$

$$\textit{inwhich} \quad t_j = t_i + j(sh/N) \tag{2}$$

Index 'j', represents the jth shifted image in the interval (exposure time). A and T are respectively the amplitude and the period of the displacement law and 'a_j' is the displacement of the object at $t=t_j$ (Fig. 3).

The next step of simulation is simply to average these generated images in order to get the ith simulated image. Again, by increasing the number of samples 'N', a better estimation of the average image is achieved.

The images generated with both of the motion simulation techniques (Sections 2.2.1 and 2.2.2) are available for download at [41] for possible analysis of other authors.

2.3. Experiments

In the second part of the study, in order to validate the simulations, a group of experimental tests are conducted. First, the same type of speckle pattern presented in Fig. 1 is attached to the surface of a planar target. Then an LSD shaker is used to vertically vibrate the target with different frequencies and amplitudes. The frequency of motion is increased from 5 to 10, 15 and 20 Hz and the amplitude of the shaker is changed from 0.5 mm (1.5 px) to 1.5 mm (4.5 px), 3 mm (9 px), 5 mm (15 px) and 7 mm (21 px). The target's motion is recorded by a digital camera with frame rate of 11, 16, 20 or 21 depending on the specific test (due to the limited frame rate of the used camera (25 fps at full resolution), the tests were done in controlled aliasing condition). The

object's position is simultaneously measured with a high resolution polytec laser interferometer. The specifications of the experimental setup are reported in Table 1.

Part of images grabbed by the camera during one cycle of the motion (starting in the static position) are shown in Fig. 4. The speckle pattern is square shaped with size of 100 mm (300 px) and average grain size of 4 px. The motion effect is more visible in neutral position, where the velocity is maximum (Fig. 4).

3. Result and discussion

In the current section, first the results of the two simulation methods are compared in the case of rigid motion and sinusoidal vibration. These results will be validated by the experimental tests.

3.1. Simulation of rigid motion with constant velocity

In order to compare the two methods of motion effect simulation in the case of rigid motion with constant velocity, two types of analyses have been performed. First, images generated numerically by each method are compared with the ones obtained from the other one. As for the second type of analysis, DIC analysis on these two groups of images is performed and the results in terms of estimated displacement and strain are compared.

Table 1
Experimental setup.

	Device	Brand and type	Specifications
1	Shaker	LSD, V830-335 TRUNNION	Max frequency =3 kHz Max mass =12 kg Max sinusoidal speed =2.0 m/s
2	Camera	AVT Marlin F131B	Equipped with a 280 × 1024 CMOS sensor Lens' nominal focal length =16 mm
3	Laser interferometer	PSV300	Single point Polytec Scanning vibrometer resolution =2.56 μm

3.1.1. Comparison of the images generated by two simulation methods

After obtaining the images with motion effect generated by each one of the two mentioned methods, two images for every motion effect index (w) are obtained. Subtracting these two images a black image should be obtained if the image generation techniques are equivalent (as expected for constant velocity target). Considering the different images obtained for w ranging from 1 to 5 px, the mean and standard deviation of the pixel intensities were found to be lower than 4×10^{-5} and 10^{-5} respectively. Since we are working with 8-bit images, the brightness values range between 0 and 255, with a brightness resolution of 1. The mentioned values of mean and standard deviation of the brightness difference are therefore many orders of magnitude lower than the brightness resolution, demonstrating that the two image generation techniques are equivalent.

3.1.2. Comparison of results after performing the DIC analysis

In the current study Vic-2D software is used in order to perform the DIC analysis. The subset size and step were set equal to 21 and 7 px respectively [1,2] (note that step=7 px corresponds to an overlap of neighbor subsets equal to 14 px). Fig. 5 gives a general sense of motion effect as the index w increases in the generated images.

By performing DIC analyses of the generated images with respect to the original one the displacement and strain values of every subset are obtained. These values have been averaged over the whole image and the results are shown in Figs. 6 and 7, in terms of mean and standard deviation of the discrepancy between the imposed and estimated motions. In these two figures only the results for $w \leq 8$ are shown because the Digital Image Correlation method is barely able to perform the matching in the generated image with w index higher than 8.

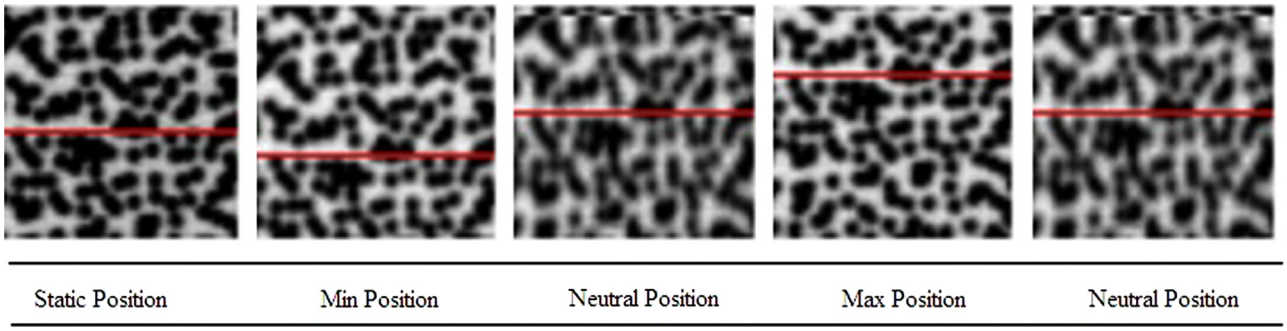

Fig. 4. A part of a typical image taken by the camera in one cycle of the motion starting and ending in static position. The red horizontal line is sketched to give better understanding of the sinusoidal vibration. (For interpretation of the references to color in this figure legend, the reader is referred to the web version of this article.)

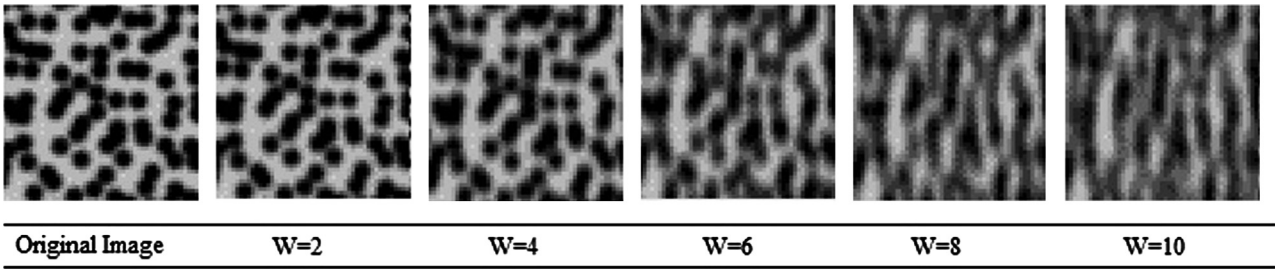

Fig. 5. Sense of motion effect as the index w of the generated images increase.

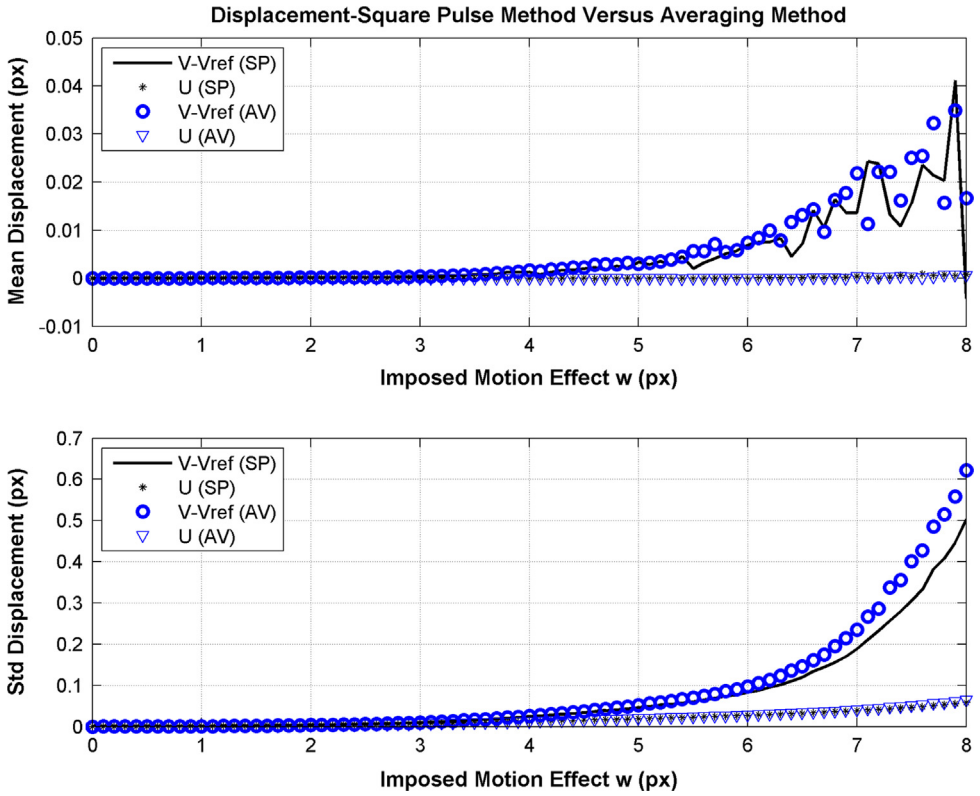

Fig. 6. Mean and standard deviation of displacement in the case of rigid motion simulation. V is the displacement in the direction of motion and Vref=0 whereas U is displacement in the direction orthogonal to the motion. 'AV' represents the averaging method and 'SP' represents the square pulse method.

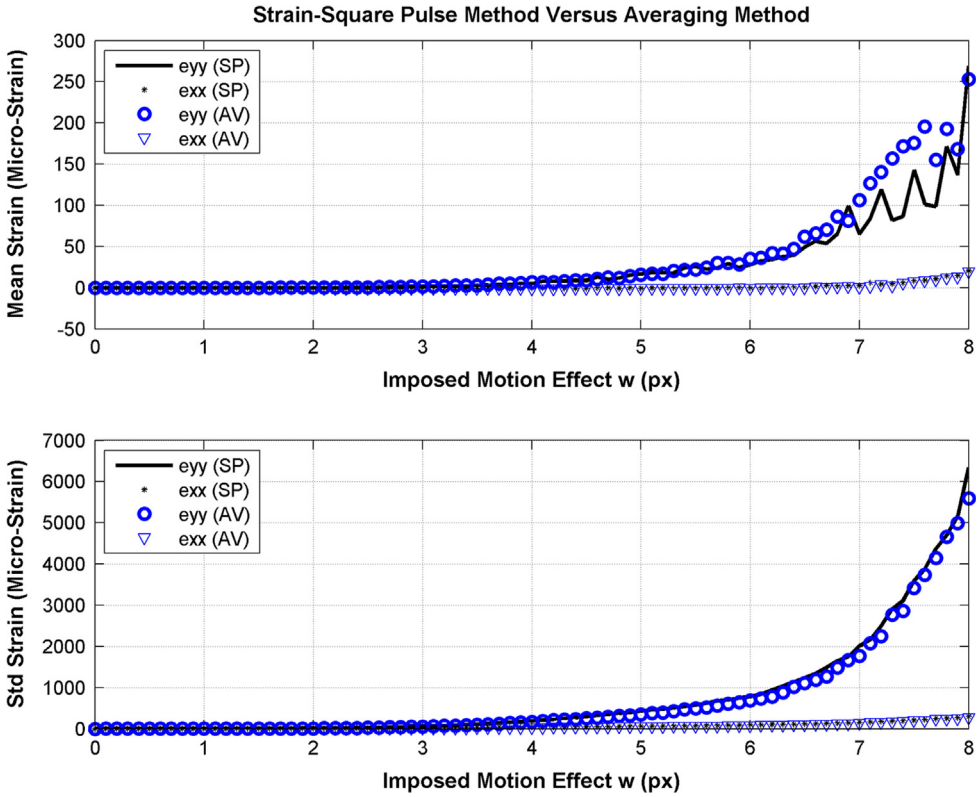

Fig. 7. Mean and standard deviation of strain in the case of rigid motion simulation. *eyy* is the strain in the direction of motion whereas. U is the strain in the orthogonal direction. 'AV' and 'SP'respectively represent the averaging method and the square pulse method.

In the case of results shown in Figs. 6 and 7, the reference mean displacement is equal to zero in both horizontal and vertical directions but since the motion effect (stripe) is simulated in vertical direction, the estimated values of displacement and strain are higher in this direction. Uncertainty values of all four parameters (*U*, *V*, *exx*, *eyy*) are considerably higher than their

corresponding mean. Therefore, it can be claimed that the uncertainty is the meaningful quantity (not mean, i.e. the average bias) that should be taken into account. In addition, up to $w=4$ px, displacement uncertainty is less than 0.025 px. Then it starts increasing with an almost constant slope ($4\text{ px} < w < 6\text{ px}$) and finally above $w=6$ px the growth rate rises considerably fast (Fig. 6). Strain uncertainty curves show similar behavior (Fig. 7) as expected, since strain is estimated relying on the displacement data as described in [12].

Figs. 6 and 7 demonstrate that in the case of rigid motion with constant velocity there is no considerable difference between estimated displacement and strain obtained by analyzing the images generated by the averaging and square pulse methods.

3.2. Experimental validation of the two generation techniques

In this section, proposed image generation techniques (averaging and square pulse) are implemented to simulate the images of a planar target with sinusoidal vibration. The procedure of image generation has already been explained in Section 2.2. As the next step, the simulated image set is analyzed with the DIC technique and the discrepancy between the imposed and the estimated time histories is utilized to estimate the measurement uncertainty. Table 2 presents the specifications of the simulated sinusoidal vibration cases. The last column is the 'maximum nominal stripe length' which can be defined as the length of the target trajectory during an exposure time (or simply the stripe length) if it has the maximum speed for the whole camera exposure time. Note that test number 5 is done in controlled aliasing condition.

In order to recreate the conditions of real tests, a zero mean Gaussian noise with standard deviation of 2.5 has been added to the images.

In order to validate the results of simulations, the simulated cases were also experimentally tested. The specifications of the experimental setup are already explained in Section 2.3. In this case, DIC estimated displacements were compared with the corresponding values measured by the laser interferometer. The result is reported in terms of discrepancy which has been defined as the difference between time histories of the displacement estimated by DIC and reference displacement (measured by laser interferometer) (Fig. 8(a)). Note that the discrepancy calculated here is a point-by-point difference; since the interferometer and camera had different reference systems; before comparing the two time histories the mean of the two signals were set to zero. Therefore, the mean value of the discrepancy is zero by definition and is not reported here. The same kind of analysis has been performed also in the case of strain and the result is presented in Fig. 8(b).

Fig. 8 shows a good agreement between the simulations and the experiments. As we expected before, the averaging method simulates better the reality in this motion condition.

Table 2
Specifications of simulated tests.

Test number	Amplitude (px)	Frequency (Hz)	Exposure time (ms)	Frame rate (frame/s)	Max nominal stripe length (px)
1	1.5	5	4	20	0.19
2	9	5	5	20	1.41
3	9	5	20	20	5.65
4	15	5	15	20	7.07
5	21	15	4	16	7.92

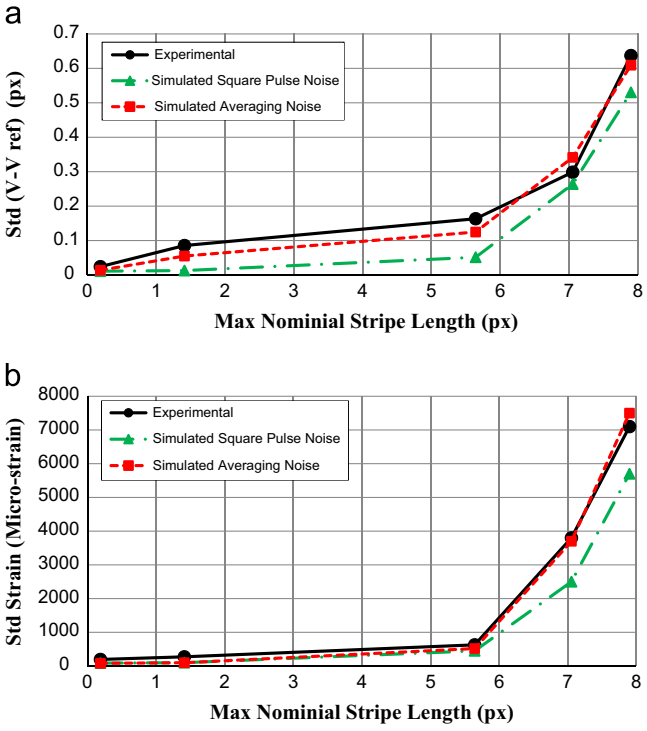

Fig. 8. Simulation of a few sinusoidal vibration tests and the corresponding experimental validation in case of (a) displacement and (b) strain estimation.

4. Deconvolution analysis for DIC uncertainty reduction

In the previous sections, the motion effect present in dynamic acquisitions has been simulated by convolving the reference image with the proper square pulse function. In the current section a deconvolution analysis is performed aiming to estimate the motion effect present in an acquired image. The final goal of this analysis is two-fold: first of all to estimate the uncertainty of the measurement relying on the estimated motion effect and second to reduce this uncertainty as detailed in Section 4.2. The deconvolution analysis can be done by considering an image of the target corrupted by motion effect and a reference (static) image of the same target and identifying the specific square pulse which could be convolved with the reference image to recreate the other one. Once the square pulse is determined, the corresponding width would be an estimation of motion effect w and the shift would represent the net displacement of the target.

4.1. Deconvolution for motion effect estimation

As described in Section 2.2.1, the motion effect can be simulated convolving the image of the fixed target with a square pulse. This corresponds to computing the product of the image Fourier Transform with the square pulse spectra. If the motion corrupted and reference (fixed) images are available, the ratio of the corresponding spectra represents the Fourier Transform of the square pulse to be identified. The detailed procedure is as follows:

(1) First of all, the Discrete Fourier Transform (DFT) of a row of the image (in the case of horizontal motion) or a column (in the case of vertical motion) is computed.
(2) The ratio of the obtained DFT with respect to the DFT of the corresponding row (or column) of the reference image needs to be found.
(3) This procedure has to be repeated for all the rows (or columns) and these results averaged. Note that, this ratio signal is in

frequency domain and is supposed to be equivalent to the DFT of a desired square pulse with known '*w*' and '*a*' parameters. The square pulse will be determined in the next two steps.

(4) Considering the fact that the Fourier Transform of a square pulse is a sinc function, determining the parameter of the square pulse could be done in frequency domain. The fourth step is to match a sinc function to the obtained ratio signal (in frequency domain).

(5) Once the sinc function is fitted, the parameters of the corresponding square pulse (width and offset) are determined.

The deconvolution technique will be implemented in two different cases: numerically generated images and experimentally acquired images.

4.1.1. Estimating motion effect in numerically generated images

As the first step to evaluate the performance of this technique for motion effect estimation, a set of shifted images with motion effect are generated using the method discussed in Section 2.2. This could be a trustable approach to check the reliability of the deconvolution analysis outcome, since the reference values of motion effect w_{ref} and shift a_{ref} of each image are known in advance. After estimation of parameters '*w*' and '*a*' by performing the deconvolution analysis, the bias error in estimation of motion effect and the corresponding shift in two cases of simulated images are presented in Fig. 9. The reference image for both cases is the one in Fig. 1. The first case is composed of images with imposed motion effect *w* ranging from 0 to 8 px with step of 0.1 px. All the images of this group have zero displacement. The second image set is generated by imposing simultaneously motion effect and shift to the reference image. The value of motion effect in the first case varies from 0 to 8 px with step of 0.1 px and the shift in each image is chosen to be twice of the corresponding *w* (shift$=2w$). As an example, the image with motion effect $w=2.1$ px has imposed shift $=4.2$ px.

According to Fig. 9, the results for the two cases of generated images are very similar. Therefore it can be claimed that the bias error in estimation of both motion effect and shift does not depend on the imposed shift value. Moreover deconvolution allows estimating the motion effect more accurately when $w>1$ (see in particular the bias error trend). The reason can be explained by considering Fig. 10. In this figure the ratio signal and the corresponding fitted sinc function are plotted for different combinations of imposed motion effect and imposed shift.

Comparing Fig. 10(a) with (b) reveals that the amplitude is not influenced by the imposed shift in the case of $w=0.5$ px. The same thing can be understood by comparing Fig. 10(c) and (d) (where $w=7.5$); therefore it can be claimed that the estimation of motion effect in the case of numerically generated images does not depend on the imposed shift value. In addition, the graphs show better fitting when it comes to higher motion effect values (Fig. 10 (c) and (d)), while in the lower motion effect cases in which the amplitude of the ratio signal is almost constant (close to 1), fluctuations in the curve due to noise can be critical and misleading for fitting the sinc function (Fig. 10(a) and (b)). This can explain the presence of the initial peek in the motion effect bias error curve (Fig. 9).

Even though the presence of the peak in motion effect bias error curve demonstrates that this technique is less accurate in the case of smaller *w* values, the accuracy is still acceptable for the purpose of this work. This statement can be explained by recalling the fact that the influence of motion effect on uncertainty of DIC is almost negligible when *w* is smaller than 1 px (Fig. 6). The real concern while implementing DIC is when the motion effect on the acquired images is significant (i.e. $w \gg 1$ px). It can be also noticed that the deconvolution analysis is even more accurate in estimation of shift than the motion effect.

4.1.2. Estimating motion effect in experimentally acquired images

Although the performance of deconvolution technique is proven to be acceptable in the case of numerically generated images

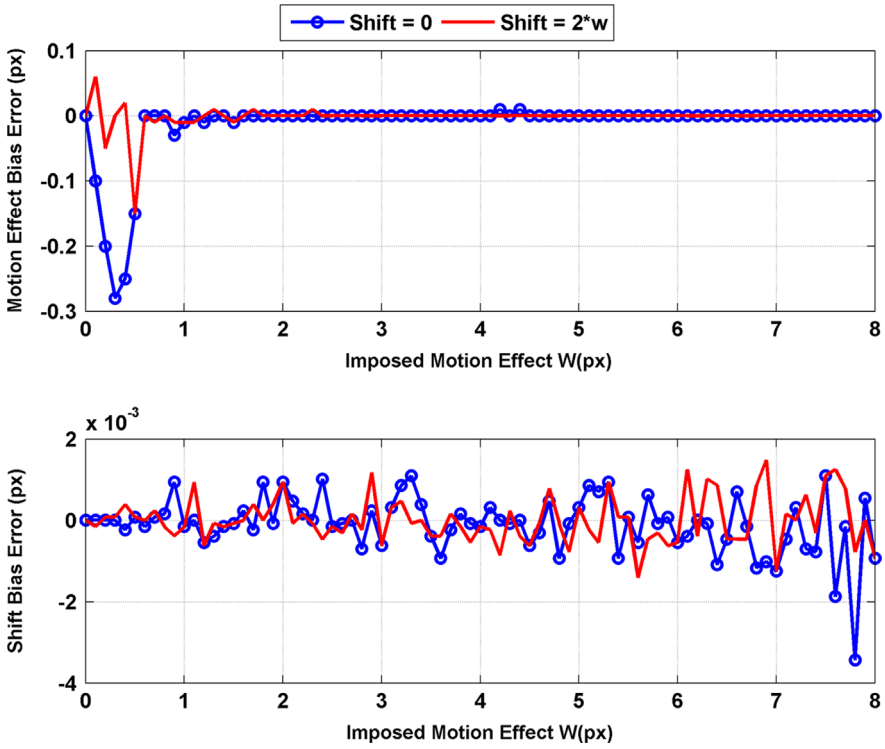

Fig. 9. Bias error in estimation of motion effect and shift in two cases of generated images with imposed *w* ranging from 0 to 8 px.

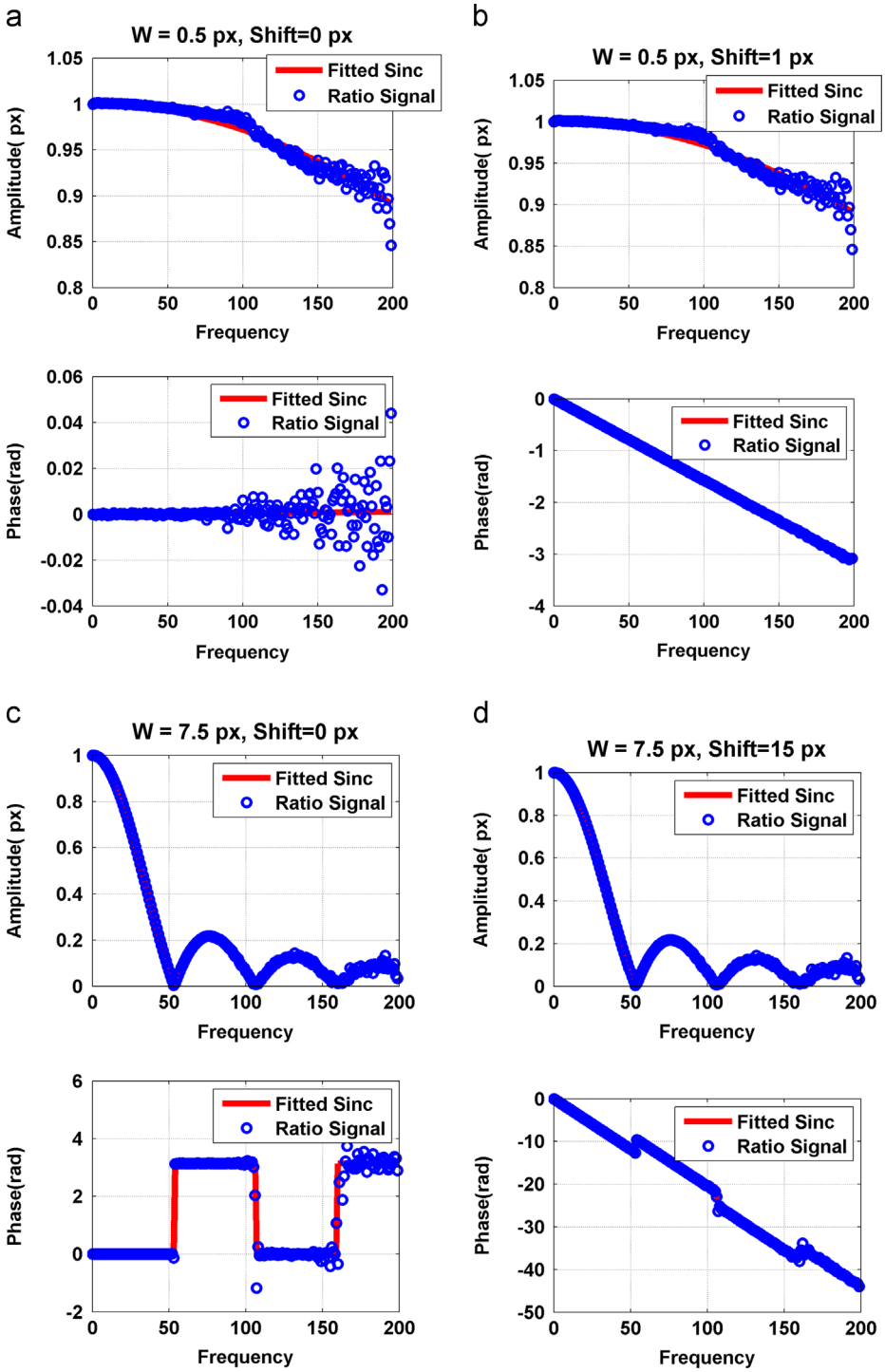

Fig. 10. Ratio signal and the corresponding fitted sinc function in frequency domain after performing the deconvolution analysis on four different generated images with (a) $w=0.5$ px, shift $=0$ px, (b) $w=0.5$ px, shift $=1.0$ px, (c) $w=7.5$ px, shift $=0$ px and (d) $w=7.5$ px, shift $=15$ px. The horizontal axis is spatial frequency that varies from zero to Nyquist frequency.

the important issue is how it performs on the images acquired in a real dynamic test. In order to answer this question the same analysis has been carried out in the case of a single sinusoidal vibration test (Table 3). For every frame of the test, the deconvolution technique has been implemented and the estimated motion effect w and the corresponding shift have been obtained.

In Fig. 11, the ratio signal and the corresponding fitted sinc function are plotted for the first frame of the experiment. Only the first lobe of the ratio signal has been used for fitting the sinc function because the matching between the two curves is better in

Table 3
Specifications of the real test.

Test data	
Frequency (Hz)	15
Amplitude	21 px (7 mm)
Exposure time (ms)	5
E2PR	0.075
Max nominal stripe length	9.87(px)
Frame rate	16

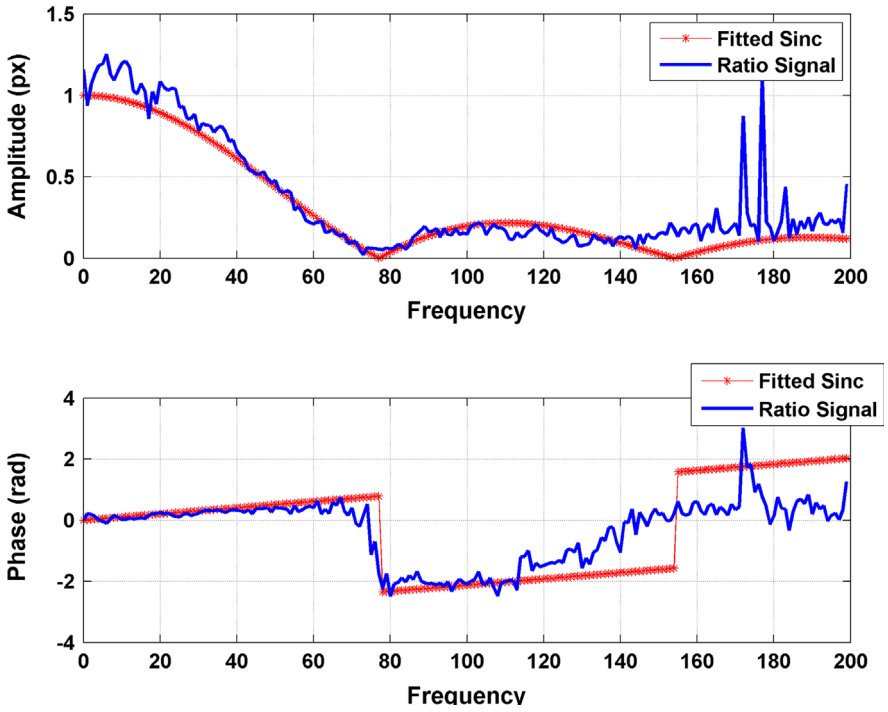

Fig. 11. Ratio signal and the corresponding fitted sinc function in frequency domain after performing the deconvolution analysis on a seventh frame of the real test. The horizontal axis is spatial frequency that varies from zero to Nyquist frequency.

Table 4
Estimated w in each frame of real test obtained by deconvolution and the corresponding reference value.

Frame	1	2	3	4	5	6	7	8	9	10	11	12	13	14	15	16	17
Estimated w (px)	9.7	9.4	7.3	4.1	1.1	4.1	7.1	8.7	9.2	9.0	6.8	4.2	1.3	3.5	6.5	8.9	9.6
Ref w (px)	9.9	9.4	7.4	3.9	0.6	3.9	7.0	8.9	9.5	8.7	6.8	3.9	0.8	3.2	6.4	8.8	9.9

the low frequency range and therefore the estimation of w is improved in this way. The same procedure has been repeated for every frame of the test and the estimated motion effect is reported in Table 4, together with the corresponding reference value.

The instantaneous position of the target during the experimental tests is known thanks to the measurement of the laser interferometer. The displacement of the target during the exposure time can therefore be estimated for each frame. This displacement value is the reference w in that particular frame (Table 4, second row). The highest motion effect values correspond to frames 1, 9 and 17 because they correspond to those moments in which the velocity of the target is the largest (zero crossing points in the sinusoidal motion). Fig. 12(a) presents the bias error in estimation of motion effect w using the deconvolution technique. According to Fig. 12(a), the bias error does not exceed 0.6 in one cycle of the motion and therefore the accuracy of this technique is in an acceptable range for the purpose of this work (see Section 4.1).

The deconvolution technique was also used to estimate the displacement of the motion. Fig. 12(b) compares this result with the laser data. This approach is able to reliably estimate the displacement as long as we are dealing with rigid motion.

4.2. Deconvlotion for improving DIC performances in dynamics

We propose in this work to use deconvolution to improve the performances of DIC in dynamics. The idea is to generate a new reference image that has the same motion effect w as the one acquired in a dynamic condition but with shift=0. Therefore the following steps below need to be done:

(1) Perform the deconvolution analysis on the ith acquired image I_i in order to determine the motion effect value w_i.
(2) Analytically convolve, using the techniques discussed in Section 2.2, the reference (fixed) image with a zero centered square pulse which has a width equal to w_i to obtain the image R_i. This new image can be considered as the new reference image for DIC analysis of image I_i.

This technique has been implemented in the case of the sinusoidal vibration test (Table 3). From the deconvolution analysis the motion effect w is already known for every frame (Table 4). As the next step, this estimated w has been used to generate the new reference image R_i for each frame I_i. Then, the DIC analysis has been carried out. It needs to be mentioned that the images in this case were 300×300 px^2, the subset size was 21 px and the overlap was 7 px. Fig. 13 compares the results of the improvement technique with that of the normal DIC and demonstrates that the proposed technique can significantly improve the displacement estimation and the corresponding standard deviation graph. Studying the discrepancy of the result reveals that with the help of deconvolution, the matching between DIC and laser interferometer measurement improves significantly, for both bias error and standard deviation (Fig. 13(a) and (b)).

As mentioned, the frames acquired when the target is crossing the neutral position are the ones with the largest values of motion effect. Therefore in Fig. 13(b) the normal DIC technique estimates

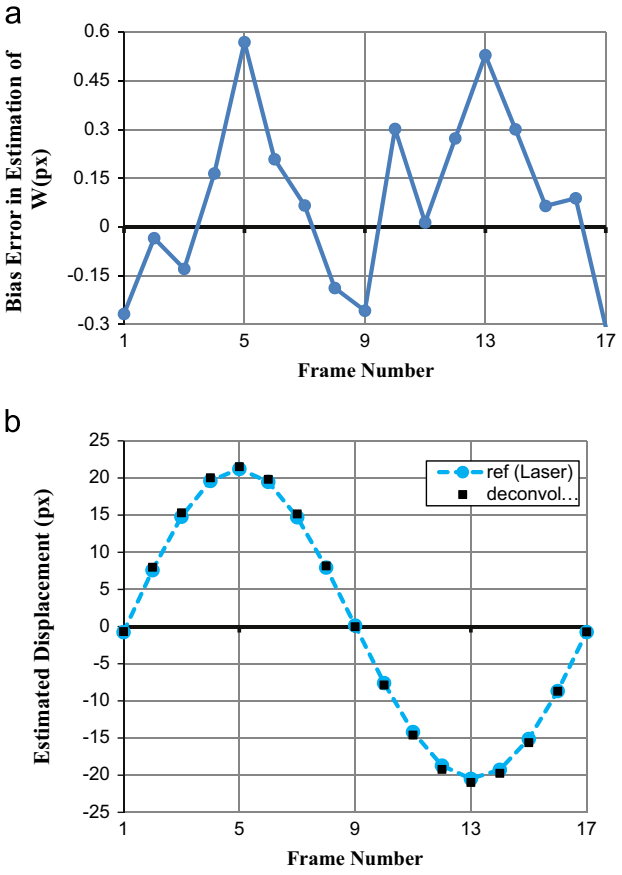

Fig.12. Using deconvolution technique to estimate (a) the motion effect *w* and (b) the corresponding displacement in the case of experimental test.

the displacement with higher uncertainty values in zero crossing frames.

5. Conclusion

In dynamics, dealing with a moving target causes a motion effect (i.e. blurring) on the acquired images. This factor is an important source of measurement uncertainty while implementing the Digital Image Correlation (DIC) technique. In the present study, the uncertainty of DIC in dynamic conditions has been evaluated and improved.

The whole work can be divided into two main parts. In the first part, two different methods to simulate the motion effect on a reference image have been proposed, discussed and validated. These methods allow simulating the acquired images in a real dynamic test and estimating the measurement uncertainty caused by the motion effect. The images generated with the technique proposed in this work are available for download at [41]. The validation has been performed by experimentally creating the simulated cases. Therefore, a harmonic motion was imposed to an object, framed by a camera, and it's position has been measured by a laser interferometer. The results show good agreement between the experiments and the simulations in terms of measurement accuracy modification in dynamic conditions.

In the second part of the study a numerical technique has been proposed to estimate the motion effect present in an acquired image. This technique gives two main advantages. First, since the motion effect itself has a known influence on the uncertainty of measurement (thanks to the first part of the study), we will be able to predict the uncertainty of DIC by just having an acquired

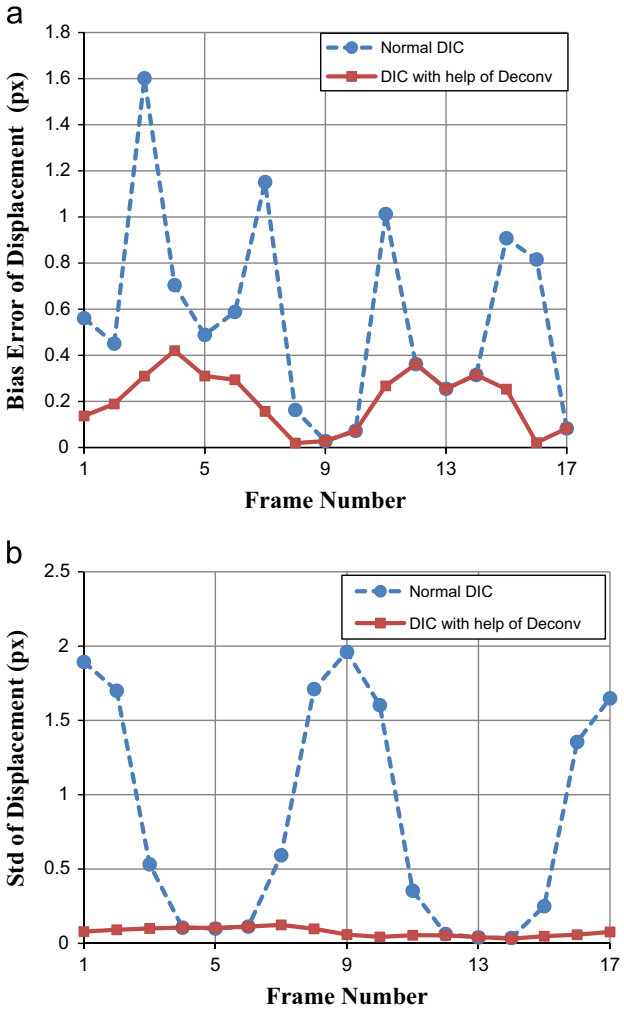

Fig. 13. (a) Bias error and (b) standard deviation of estimated displacement in every frame of the real test.

image. Second, this numerical technique was used to improve the performances of DIC in dynamic applications. In this way the bias error and the uncertainty of measurements were considerably decreased.

References

[1] Sutton MA, Orteu JJ, Schreier HW. Image correlation for shape, motion and deformation measurements: basic concepts, theory and applications. Springer, New York; 2009.

[2] Pan B, Qian K, Xie H, Asundi A. Two-dimensional digital image correlation for in-plane displacement and strain measurement: a review. Meas Sci Technol 2009;20:062001.

[3] Schmidt T, Tyson J, Galanulis K. Full-field dynamic displacement and strain measurement using advanced 3D image correlation photogrammetry. Exp Tech 2003;27(3):47–50.

[4] Wang X, Yi T, Tang Q, Feng L, Ni G, Zhou L. Simulation and analysis of vibration blurred images, In: Proceedings of the wireless communications networking and mobile computing conference IEEE 2010 1–4.

[5] Schreier HW, Sutton MA. Systematic errors in digital image correlation due to undermatched subset shape functions. Exp Mech 2002;42(3):303–10.

[6] Siebert T, Becker T, Spiltthof K, Neumann I, Krupka R. High-speed digital image correlation: error estimations and applications. Opt Eng 2007;46(5):051004.

[7] Tiwari V, Sutton MA, McNeill SR. Assessment of high speed imaging systems for 2D and 3D deformation measurements: methodology development and validation. Exp Mech 2007;47:561–79.

[8] Um GJ, Kim H. Experimental error assessment for image correlation analysis on a paper tensile specimen. J Ind Eng Chem 2007;13(2):214–8.

[9] Haddadi H, Belhabib S. Use of rigid-body motion for the investigation and estimation of the measurement errors related to digital image correlation technique. Opt Laser Eng 2008;46:185–96.

[10] Pan B, Qian K, Xie H, Asundi A. On errors of digital image correlation due to speckle patterns, In: Proceedings of the international conference on experimental mechanics, 2008 z1–z7.
[11] Vassolera JM, Fancelloa EA. Error analysis of the digital image correlation method. Mec Comput 2010;24:6149–61.
[12] Fazzini M, Mistou S, Dalverny O, Robert L. Study of image characteristics on digital image correlation error assessment. Opt Laser Eng 2010;48:335–9.
[13] Hu Z, Xie H, Lu J, Wang H, Zhu J. Error evaluation technique for three-dimensional digital image correlation. Appl Opt 2011;50(33):6239–47.
[14] Zappa E, Mazzoleni P, Matinmanesh A. Uncertainty assessment of digital image correlation method in dynamic applications. Opt Laser Eng 2014;56:140–51.
[15] Schreier HW, Braasch JR, Sutton MA. Systematic errors in digital image correlation caused by intensity interpolation. Opt Eng 2000;39(11):2915–21.
[16] Wang ZY, Li HQ, Tong JW, Ruan JT. Statistical analysis of the effect of intensity pattern noise on the displacement measurement precision of digital image correlation using self-correlated images. Exp Mech 2007;47:701–7.
[17] Reu PL, Sutton MA, Wang Y, Miller TJ. Uncertainty quantification for digital image correlation In: Proceedings of the SEM annual conference, Albuquerque, New Mexico, USA, 2009.
[18] Wang YQ, Sutton MA, Reu PL, Miller TJ. Image matching error assessment in digital image correlation, In: Proceedings of the SEM annual conference, Albuquerque, New Mexico, USA, 2009.
[19] Wang YQ, Sutton MA, Bruck HA, Schreier HW. Quantitative error assessment in pattern matching: effects of intensity pattern noise, interpolation, strain and image contrast on motion measurements. Strain 2009;45:160–78.
[20] Wang YQ, Sutton MA, Ke XD, Schreier HW, Reu PL, Miller TJ. On error assessment in stereo-based deformation measurements part I: theoretical developments for quantitative estimates. Exp Mech 2011;51:405–22.
[21] Ke XD, Schreier HW, Sutton MA, Wang YQ. Error assessment in stereo-based deformation measurements part II: experimental validation of uncertainty and bias estimates. Exp Mech 2011;51:423–41.
[22] Bornert M, Brémand F, Doumalin P, Dupre JC, Fazzini M, Grediac M, et al. Assessment of digital image correlation measurement errors: methodology and results. Exp Mech 2009;49(3):353–70.
[23] Lava P, Cooreman S, Coppieters S, De Strycker M, Debruyne D. Assessment of measuring errors in DIC using deformation fields generated by plastic FEA. Opt Laser Eng 2009;47:747–53.
[24] Lava P, Coppieters S, Wang Y, Van Houtte P, Debruyne D. Error estimation in measuring strain fields with DIC on planar sheet metal specimens with a non-perpendicular camera alignment. Opt Laser Eng 2011;49:57–65.
[25] Lava P, Cooreman S, Debruyne D. Study of systematic errors in strain fields obtained via DIC using heterogeneous deformation generated by plastic FEA. Opt Laser Eng 2010;48:457–68.
[26] Wang Y, Lava P, Coppieters S, De Strycker M, Van Houtte P, Debruyne D. Investigation of the uncertainty of DIC under heterogeneous strain states with numerical tests. Strain 2012;48(6):1–10.
[27] Schmidt T, Tyson J, Galanulis K. Full-field dynamic displacement and strain measurement—specific examples using advanced 3D image correlation photogrametery: part1. Exp Tech 2003;26:47–50.
[28] Schmidt T, Tyson J, Galanulis K. Full-field dynamic displacement and strain measurement—specific examples using advanced 3D image correlation photogrammetery: part 2. Exp Tech 2003;27:22–6.
[29] Kirugulige MS, Tippur HV, Denney TS. Measurement of transient deformations using digital image correlation method and high-speed photography: application to dynamic fracture. Appl Opt 2007;46(22):5083–96.
[30] Wang W, Mottershead JE, Mares C. Vibration mode shape recognition using image processing. J Sound Vib 2009;326:909–38.
[31] Siebert T, Wood R, Splitthof K. High speed image correlation for vibration analysis. J Phys: Conf Ser 2009;181:1–8.
[32] Siebert T, Crompton MJ. Application of high speed digital image correlation for vibration mode shape analysis In: Proceedings of the SEM annual conference, June 2010 Indianapolis, Indiana, USA.
[33] Wang W, Mottershead JE, Ihle A, Siebert T, Reinhard Schubach H. Finite element model updating from full-field vibration measurement using digital image correlation. J Sound Vib 2011;330:1599–620.
[34] Helfrick MN, Niezrecki C, Avitabile P, Schmidt T. 3D digital image correlation methods for full-field vibration measurement. Mech Syst Signal Process 2011;25:917–27.
[35] Warren C, Niezrecki C, Avitabile P, Pingle P. Comparison of FRF measurements and mode shapes determined using optically image based, laser, and accelerometer measurements. Mech Syst Signal Process 2011;25:2191–202.
[36] Wang W, Mottershead JE, Siebert T, Pipino A. Frequency response functions of shape features from full-field vibration measurements using digital image correlation. Mech Syst Signal Process 2012;28:333–47.
[37] Patterson EA, Hack E, Brailly P, Burguete RL, Saleem Q, Siebert T, et al. Calibration and evaluation of optical systems for full-field strain measurement. J Opt Lasers Eng 2007;45(5):550–64.
[38] Davighi A, Burguete R, Feligiotti M, Hack E, James S, Patterson E, et al. The development of a reference material for calibration of full-field optical measurement systems for dynamic deformation measurements. Appl Mech Mater 2011;70:33–8.
[39] Hack E, Lampeas G, Mottershead J, Patterson E, Siebert T Whelan M. Progress in developing a standard for dynamic strain analysis In: Experimental and Applied Mechanics, Proceedings of the Society for Experimental Mechanics Series 9999, 6425–29 , doi:10.1007/978-1-4614-0222-0_52.
[40] Reu PL. Experimental and numerical methods for exact subpixel shifting. Exp Mech 2011;51:443–52.
[41] ⟨http://people.mecc.polimi.it/zappa/DIC⟩, 2014.